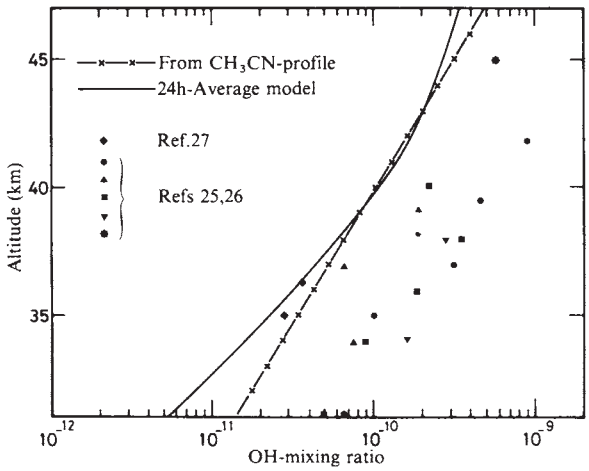

Fig. 3 OH volume mixing ratio profile calculated assuming that X were CH_3CN, and compared with measurements and model calculations. Data for 24-h average model from G. Brasseur (personal communication).

obtained OH profile is compared with recent measurements, performed by different authors[25–27].

As can be seen the OH mixing ratios of this work are considerably lower than the measurements. Note, however, that the measurements represent instantaneous values of [OH], whereas the data calculated here are 24 h averages, taking into account the long lifetime of CH_3CN versus the OH reactions (between 400 and 1,000 h for the altitude region under consideration).

In fact, a comparison of the OH profile calculated from the CH_3CN profile with a recent model calculation of the 24-h average of OH according to G. Brasseur (personal communication) turns out to be quite satisfactory, in view of the simple CH_3CN profile assumed (a straight line on semi-log plot). The reasonable agreement of these OH data with previous work can be considered as additional evidence for the identification of X as CH_3CN.

A more complete model of CH_3CN, taking into account possible surface sources, washout in the troposphere, diffusion and photochemical destruction is clearly needed to elucidate this problem. At present, however, the available data seem to indicate that the molecule X is indeed CH_3CN.

We thank the technical staffs of the Belgian Institute for Space Aeronomy and the CNES launching base at Aire-sur-l'Adour which made the experiments possible; also Dr Vrignault and the technical staff of the Centre d'Essais des Landes for the radar tracking during the balloon flight and Dr M. Ackerman for organizing the joint flight. Part of this project was financed by the NFWO (Belgian National Science Foundation) as project no. 2.0009.79.

Received 24 January; accepted 22 March 1983.

1. Mohnen, V. A. *Pure appl. Geophys.* **84,** 114–153 (1971).
2. Ferguson, E. E. in *Natural Stratosphere of 1974* (CIAP Monogr. 1, 5.42–5.54, 1974).
3. Arnold, F., Krankowsky, D. & Marien, K. H. *Nature* **267,** 30–32 (1977).
4. Arijs, E., Ingels, J. & Nevejans, D. *Nature* **271,** 642–644 (1978).
5. Arnold, F., Bohringer, H. & Henschen, G. *Geophys. Res. Lett.* **5,** 653–656 (1978).
6. Henschen, G. & Arnold, F. *Geophys. Res. Lett.* **8,** 999–1001 (1981).
7. Arijs, E., Nevejans, D., Ingels, J. & Frederick, P. *Annales Geophysicae* **1,** 163–168 (1983).
8. Ferguson, E. E. *Geophys. Res. Lett.* **5,** 1035–1038 (1978).
9. Murad, E. & Swider, W. *Geophys. Res. Lett.* **6,** 929–932 (1979).
10. Arijs, E., Nevejans, D. & Ingels, J. *Nature* **288,** 684–686 (1980).
11. Arnold, F., Henschen, G. & Ferguson, E. E. *Planet. Space Sci.* **29,** 185–193 (1981).
12. Arijs, E., Nevejans, D. & Ingels, J. *J. atmos. terr. Phys.* **44,** 681–694 (1982).
13. Bohringer, H. & Arnold, F. *Nature* **290,** 321–322 (1981).
14. Smith, D., Adams, N. G. & Alge, E. *Planet. Space Sci.* **4,** 449–454 (1981).
15. Ingels, J., Arijs, E., Nevejans, D., Forth, H. J. & Schaefer, G. *Rev. scient. Instrum.* **49,** 782–784 (1978).
16. Heaps, M. G. *Planet. Space Sci.* **26,** 513–517 (1978).
17. Rosen, J. M. & Hofman, D. J. *J. Geophys. Res.* **86,** 7406–7420 (1981).
18. Smith, D. & Adams, N. G. *Geophys. Res. Lett.* **9,** 1085–1087 (1982).
19. Bates, D. R. *Planet. Space Sci.* **30,** 1275–1282 (1982).
20. Becker, K. M. & Ionescu, A. *Geophys. Res. Lett.* **9,** 1349–1351 (1982).
21. Herzberg, G. & Scheibe, G. *Z. phys. Chem.* **B7,** 390–394 (1930).
22. McElcheran, D. E., Wynen, M. H. J. & Steacie, D. W. R. *Can. J. Chem.* **36,** 321–329 (1958).
23. Harris, G. W., Kleindienst, T. E. & Pitts, J. N. *Chem. phys. Lett.* **80,** 479–483 (1981).
24. Brasseur, G., De Rudder A. & Roucour, A. in *Proc. int. Conf. Environmental Pollution*, Thessaloniki, 839–910 (1982).
25. Anderson, J. G. *Geophys. Res. Lett.* **3,** 165–168 (1976).
26. Anderson, J. G. in *Proc. NATO Advances Study Institute on Atmospheric Ozone*, FAA-EE-80-20, 253–251 (1981).
27. Heaps, W. S. & McGee, T. J. *J. geophys. Res.* (submitted); *The Stratosphere 1981, Theory and Measurements*, 1–105 (WMO Rep. No. 11, 1981).

Direct surface imaging in small metal particles

L. D. Marks

Cavendish Laboratory, Madingley Road, Cambridge CB3 0HE, UK

David J. Smith

High Resolution Electron Microscope, University of Cambridge, Free School Lane, Cambridge CB2 3RQ, UK

Atomic-level information about the surfaces of small metal particles has been recorded directly in recent observations with a 600-kV high-resolution electron microscope. Here, we have studied small polycrystalline particles of silver and gold tilted to bring their surfaces parallel to the electron beam. However, unlike previous workers using this normal reflection electron microscopy (REM) configuration, we have used conventional bright field axial imaging thereby considerably facilitating image interpretation. As well as clean, sharp surface images, morphological details of catalytic significance, such as the distribution of surface steps, particle facetting and the nature of surface reconstructions, have been obtained. Moreover, detailed computer simulations confirmed that the electron micrographs can be interpreted in terms of atomic columns and, in particular, established that some micrographs showed, for the first time in a transmission electron microscope (TEM), direct atomic-scale imaging of a reconstructed metal surface.

The first direct atomic imaging in the electron microscope was achieved by Crewe and co-workers using the scanning transmission instrument[1], and several workers[2,3], have demonstrated that imaging of atoms is feasible, although less straightforward, in the conventional TEM using tilted-beam dark-field illumination. Good quantitative agreement between experimental bright-field images of isolated tungsten atoms and clusters with calculated contrast levels has also been obtained[4]. Furthermore, it is possible to obtain images of crystals showing surface information on the atomic scale. For example, surface steps in projection have been observed[5] in MgO and gold[6] in weak-beam dark-field imaging conditions and also in gold[7] using forbidden reflections, whilst single atomic steps on the (111) surface of silicon crystals were imaged using a bright field technique[8]. Cowley has used the scanning TEM in a glancing incidence surface imaging mode[9] to observe unit-cell-high steps on the faces of MgO crystals. This REM technique, which utilizes electrons incident at glancing angles (and thereby produces a severely foreshortened image) has also been used to good effect in TEM studies of surface topography. Direct observations, for example, of superstructures in silicon resulting from surface reconstruction have been made[10]. The various configurations and results for surface imaging have been recently reviewed[11].

The specimens of silver and gold were prepared by evaporation and epitaxial growth on heated alkali halide substrates, as described elsewhere[12]. These were examined at either 500 or 575 kV using the Cambridge University high-resolution electron microscope (HREM)[13]; recent modifications and increased resolution[14] have resulted in almost an order of magnitude improvement in the signal-to-noise ratios for the common lattice spacings (0.235 nm for 111 beams and 0.204 nm for 200) and experimental imaging conditions could be accurately chosen by direct particle observation using an image pick-up

0028-0836/83/210316—02$01.00

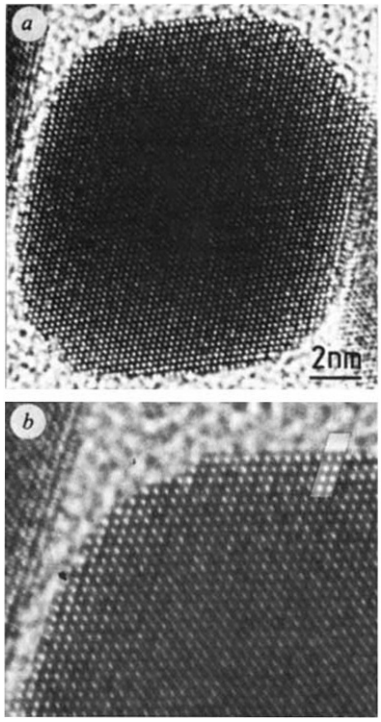

Fig. 1 *a*, High-resolution electron micrograph of a small, slightly-rounded, square-pyramidal particle of gold after tilting from the ⟨100⟩ epitaxial orientation to the ⟨110⟩ pole. Visible lattice spacings are 0.235 nm and 0.204 nm. Reverse contrast image–atomic columns appear white. *b*, Enlargement from *a*, with image simulation superimposed. Note visibility of surface steps and facetting.

and viewing system[15]. Theoretical calculations, used for confirmation of the image interpretations, were carried out using computer programs based on the multi-slice approach[16,17]. However, because of the step discontinuity between the finite-thickness crystal and vacuum, as well as periodic continuation effects[18], obtaining a good fit at the edge of the crystal was not simple (L.D.M., in preparation). The standard resolution-limiting factors of energy spread and beam convergence were included by an incoherent image summation in real space rather than the more usual reciprocal space envelope function approach.

In both the experimental and theoretical images we have concentrated, for convenience, on the ⟨110⟩ pole, although we have some preliminary images which indicate that our results and conclusions are applicable in other projections. Our results are illustrated by Fig. 1, which is an image of a slightly-rounded square pyramid of gold tilted from its original ⟨100⟩ epitaxial orientation to the ⟨110⟩ pole. Figure 1*a* shows the entire particle whilst Fig. 1*b* shows an enlargement of its top edge together with the results of a numerical image simulation for a $\langle 1\bar{1}1\rangle$ surface of a crystal of constant thickness. At this particular objective lens defocus (−97.5 nm), the white spots in both the calculated and experimental images can be interpreted directly as columns of atoms; surface steps and facetting are clearly visible.

The power of the technique for examining surfaces is well demonstrated by Fig. 2. This image, which was recorded at the optimum defocus (atomic columns black), shows a $\langle 1\bar{1}1\rangle$ surface of a gold particle which has partially reconstructed to a (2×1) surface (that is, a surface with a double periodicity in the ⟨001⟩ direction). Such reconstructed surfaces are well known from macroscopic surface techniques but have never been imaged directly in previous electron microscopy observations. Although there is some surface roughness, and the reconstruction is irregular, part of the edge of the particle provides unambiguous evidence for the 'missing-row' model for this

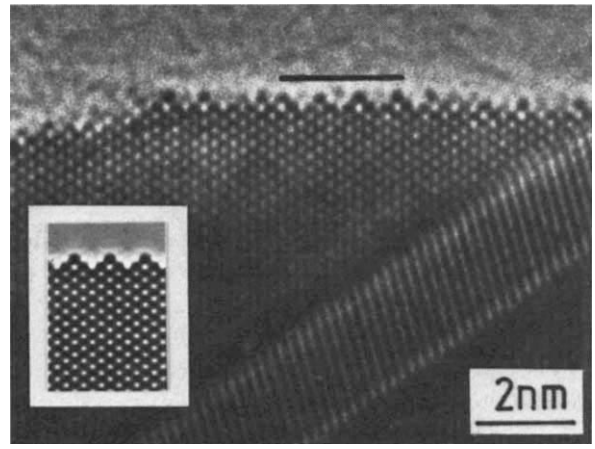

Fig. 2 Small particle of gold showing directly, at the atomic level, a partially-reconstructed (2×1) surface superstructure. Inset shows a calculated image, corresponding to the so-called 'missing-row' model[20], which matches well with the experimental image in the region marked.

reconstructed surface[19] (that is, the loss of every second column of atoms on the surface) as shown by comparison with the calculated image inset. Independent confirmatory evidence for this missing-row model has also been recently obtained using scanning tunnelling microscopy[20]. Further observations and image simulations, which will be described in detail elsewhere (work in preparation), establish that such surface images are indeed sensitive to the chemical nature of the surface; as shown by the inset, for example, we are faithfully imaging the gold surface rather than contamination atoms.

Knowledge of the structure and composition of solid surfaces is essential to a proper understanding of many physical and chemical properties. Moreover, it is the surfaces of small metal particles which are crucial in determining the behaviour of many heterogeneous catalysts. Our results clearly demonstrate that the surface structure of small metal particles can now be directly characterized with atomic resolution in the electron microscope; that is, local structural information is provided which is comparable with the macroscopic results produced by low-energy electron diffraction (LEED) techniques. Admittedly, we have used an idealized model system but other f.c.c. metals are known to have similar particle structure and comparable effects have already been seen in preliminary observations of Pt-impregnated graphite industrial catalysts (E. Noordally and L. A. Freeman, personal communication). Fundamental insights into the structural aspects of heterogeneous catalysis can be expected from a detailed exploitation of this technique.

This work has been supported by the SERC.

Received 17 January; accepted 8 March 1983.

1. Crewe, A. V., Wall, J. & Langmore, J. *Science* **168,** 1338–1340 (1970).
2. Hashimoto, H. *et al. Jap. J. appl. Phys.* **10,** 1115–1116 (1971).
3. Dorignac, D. & Jouffrey, B. *J. Microsc. Spectrosc. Electron* **5,** 671–680 (1980).
4. Iijima, S. *Optik* **48,** 193–214 (1977).
5. Kambe, K. & Lehmpfuhl, G. *Optik* **42,** 187–194 (1975).
6. Yagi, K. *et al. Surface Sci.* **86,** 174–181 (1979).
7. Cherns, D. *Phil. Mag.* **30,** 549–556 (1974).
8. Iijima, S. *Ultramicroscopy* **6,** 41–52 (1981).
9. Cowley, J. M. in *Proc. 39th A. EMSA Meet.* (ed. Bailey, G. W.) 212–215 (Claitors, Baton Rouge, 1981).
10. Osakabe, N., Tanishiro, Y., Yagi, K. & Honjo, G. *Surface Sci.* **109,** 353–366 (1981).
11. Takayanagi, K. in *Electron Microscopy 1982* Vol. 1, 43–50 (Deutsche Gesellschaft für Elektronenmikroskopie e.V., Frankfurt, 1982).
12. Marks, L. D. & Smith, D. J. *J. Cryst. Growth* **54,** 425–432 (1981).
13. Smith, D. J. *et al. Ultramicroscopy* **9,** 203–214 (1982).
14. Smith, D. J. *et al. J. Microsc.* **130,** 127 (1983).
15. Catto, C. J. D. *et al.* in *Electron Microscopy and Analysis 1981* (ed. Goringe, M. J.) 123–126 (Institute of Physics, Bristol, 1982).
16. Cowley, J. M. & Moodie, A. F. *Acta crystallogr.* **10,** 609–619 (1957).
17. Goodman, P. & Moodie, A. F. *Acta crystallogr.* **30,** 280–290 (1974).
18. Wilson, A. R. & Spargo, A. E. C. *Phil. Mag.* **46,** 435–449 (1982).
19. Bonzel, H. P. & Ferrer, S. *Surface Sci.* **118,** L263–L268 (1982).
20. Binnig, G., Rohrer, H., Gerber, C. & Weibel, E. *Phys. Rev. Lett.* (submitted).